Note: Snapshot PDF is the proof copy of corrections marked in EditGenie, the layout would be different from typeset PDF and EditGenie editing view.

Author Queries & Comments:

Q1 : The disclosure statement has been inserted. Please correct if this is inaccurate.

Response: The statement is ok

An experimental-numerical method for the prediction of on-road comfort of city bicycles

Recto running head : VEHICLE SYSTEM DYNAMICS

Verso running head : A. DORIA ET AL.

Alberto Doria[a], Edoardo Marconi[a], Luis Munoz[b], Alejandra Polanco[c], Daniel Suarez[c]

[a]Department of Industrial Engineering, University of Padova, Padova, Italy

[b]Department of Mechanical Engineering, Universidad de los Andes, Bogotá, Colombia

[c]Department of Industrial Engineering, Pontificia Universidad Javeriana, Bogotá, Colombia

CONTACT Alberto Doria alberto.doria@unipd.it

History : received : 2019-05-29 revised : 2020-03-23 accepted : 2020-04-01

ABSTRACT

A low-cost experimental-numerical method for the prediction of on-road comfort of city bicycles is presented. Experimental tests are performed by exciting the wheels of the bicycle with impulsive vibrations and measuring the frequency response functions (FRFs) between different sensitive points of the bicycle (*i.e.* seatpost and steerer tube) and the wheels. Laboratory tests are carried out with the rider on the bicycle, and the posture is carefully checked. A mathematical model is employed to predict the accelerations experienced by the rider on the road, considering tyre and wheelbase filtering. As a verification of the proposed methodology, comfort predictions obtained with the experimental-numerical method are compared with reference data obtained from road tests. A general agreement in terms of the root mean square values and power spectral densities is found.

KEYWORDS

- Bicycle
- comfort
- vibrations
- impulsive testing
- ride comfort evaluation

Introduction

Nowadays, the study of bicycle comfort is an interesting research topic closely related to sustainable mobility, as the problem of low-emission urban and sub-urban mobility is often solved through a widespread use of bicycles and bicycle lanes. City bicycles are used by a wide range of people, including kids, elders, and workers that use the bicycle throughout the day. For some of these users, ride comfort may be an important issue, and the continuous use of an uncomfortable bicycle may lead to back pain or other disorders.

Bicycle comfort depends on many mechanical, biomechanical, and environmental factors [1], including the level of vibrations transmitted to the rider, the posture, the distribution and amplitude of contact forces between the rider and the vehicle, traffic and weather conditions. Nevertheless, most researchers recognise the vibrations transmitted to the cyclist as one of the main causes of discomfort [2–4]. For this reason, some studies dealing with bicycle vibrations have already been carried out.

Some researchers performed specific road tests installing a data logger or a computer on the bicycle and measuring the vibrations of the handlebar, saddle, and other relevant points using accelerometers [2,5,6]. The analysis of road tests results in the

frequency domain [2,5] showed that most of the vibrations caused by road excitation belong to the 0-60 Hz band and that in this band the spectra are very irregular, with a large number of close peaks.

Even if road tests are the most direct method for measuring bicycle comfort, some researchers highlighted that the repeatability of results is sometimes poor, owing to variations in rider posture, bicycle speed, and road conditions [7]. Consequently, some laboratories developed indoor testing equipment, based on shakers [8,9] that mimic road excitations, to systematically analyse the relative contribution of bicycle components to the vibrations transmitted to the cyclists. However, the test benches equipped with shakers are rather expensive and require particular structures and connections between the shaker and the vehicle under testing [10].

A valid alternative to shaker tests is the identification of the frequency response functions (FRFs) of the bicycle-rider system with the impulsive method [11,12] and the prediction of vibrations on the road using an experimentally-derived bicycle model and normalised road profiles [13].

In recent years some factors have promoted the development of testing methods based on impulsive excitation. For example, the basic equipment (which includes an instrumented hammer, an accelerometer, a DAQ board, and a computer) is nowadays affordable for most laboratories and bicycle manufacturers. Also, the software currently available makes it possible to perform sophisticated elaborations of experimental results, and interesting information can be found both in the frequency and the time domain.

This paper presents a new low-cost testing method for the prediction of the vibrations experienced by the cyclist on the road, starting from indoor tests carried out with the impulsive technique. The testing method was developed making use of simple equipment and carefully controlling the testing conditions. The method was designed for normal riding on a city bicycle lane.

The next section presents the theoretical background of the mathematical model for the elaboration of the FRFs measured indoor and the prediction of vibrations on the road. Two important effects are considered: wheelbase filtering [14] and tyre filtering [15]. The third section deals with equipment and methods adopted to carry out the indoor and road tests for validating the proposed method. A diamond-frame bicycle and a step-through-frame bicycle are considered. Sensitive points and measurement directions are presented. In the fourth section, the FRFs measured indoor are reported, discussed, and elaborated to predict vibrations on the road. The fifth section deals with road tests, power spectral densities (PSDs) of acceleration components of sensitive points are presented and discussed. The comparison between the vibrations predicted by laboratory tests and the vibrations measured on the road is presented in the sixth section. PSDs and root mean square (RMS) values are compared. Finally, conclusions are drawn.

Theoretical background

Tyre-road vertical interaction

The vertical interaction of a tyre with an uneven road is a complex phenomenon that involves the deformation of the road, the geometric tyre-road interaction, the flexibility of the tyre, and the tyre tread pattern (especially in off-road cycling). Several models of this interaction have been developed, dealing with different parts of the whole phenomenon [15–20]. In the case of a city bicycle, it is reasonable to make some assumptions: the bicycle is ridden on-road, hence, the tyre sinking is negligible; the road profile can be represented as a Gaussian process, and there are no cleats, bumps, or other abrupt obstacles in the road; there are no severe turning or braking actions during riding, hence, shear stresses in the contact patch are negligible. As there is no tyre sinking, a rigid road can be used in the model [16,20]. Given the assumption that the road profile is a Gaussian process, it can be described by means of a power spectral density (PSD) [21]. As there are no abrupt discrete obstacles, the interaction between the road and the tyre can be modelled considering only the flexibility of the tyre, neglecting the geometric enveloping effect [17,20].

Under these conditions, the flexible interaction can be represented as a filter applied to the original road profile $q(X)$, generating an effective road profile $q_e(X)$. This effect can be modelled by the surface contact model presented in [15]. This model belongs to a family of models focused on tyre flexibility, simplifying the contact with a fixed contact area [20,22]. The road surface profile $q(X+x)$ is defined over a constant and symmetric contact patch with length $2a$ as a function of X (the rolling distance, *i.e.* the absolute longitudinal coordinate of the wheel centre) and x (the longitudinal coordinate relative to the wheel centre). Figure 1 shows the real flexible tyre excited by the road surface profile $q(X+x)$ and the equivalent system composed of a spring excited by the effective road profile $q_e(X)$. The tyre dynamic vertical force acting on the real tyre is given by:

$$F_{zd}(X) = \int_{-a}^{a} c_t(x)[q(X+x) - \zeta(X)]\,dx \tag{1}$$

where $c_t(x)$ is the distributed tyre vertical stiffness and $\zeta(X)$ is the vertical displacement of the wheel centre.

Figure 1. Tyre filtering: surface contact model.

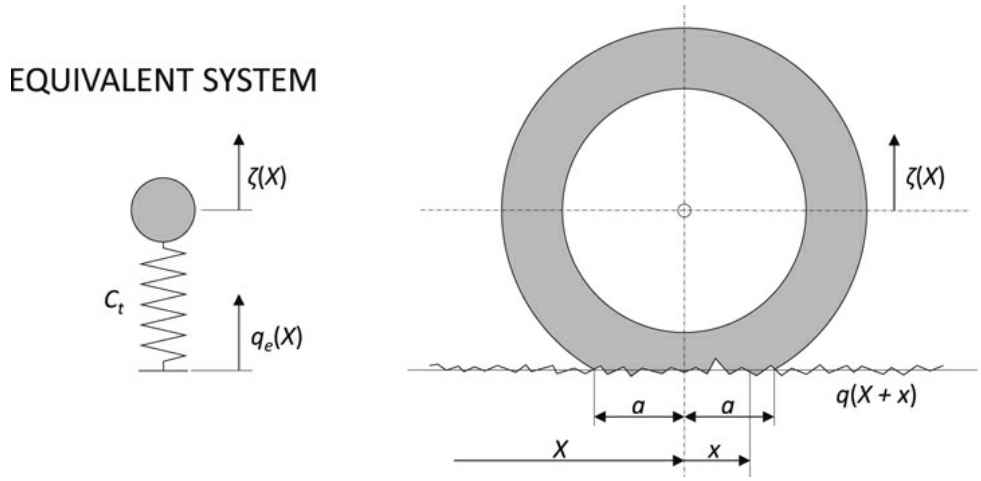

In the equivalent system, the effective road profile must satisfy

$$F_{zd}(X) = C_t[q_e(X) - \zeta(X)] \tag{2}$$

where C_t is tyre nominal vertical stiffness or integral vertical stiffness.

Comparing Equation (1) and (2), the following expression of the effective road profile $q_e(X)$ as a function of the nominal road profile $q(X)$ can be obtained:

$$q_e(X) = \frac{\int_{-a}^{a} c_t(x) q(X+x) dx}{C_t} \tag{3}$$

This is the expression of a weighted moving average filter that uses the distributed vertical stiffness as weighting function and the length of the contact patch as averaging window. In the simple case here considered, in which the distributed stiffness is assumed constant along the contact patch ($c_t(x) = C_t/2a$), the filter becomes a simple moving average:

$$q_e(X) = \frac{1}{2a}\int_{-a}^{a} q(X+x) dx \tag{4}$$

Equation (4) can be rewritten using the absolute coordinate system:

$$q_e(X) = \frac{1}{2a}\int_{X-a}^{X+a} q(\tilde{X}) d\tilde{X} \tag{5}$$

In order to obtain the effective road profile from standardised PSDs, it is necessary to derive the transfer function of the moving average filter in the angular-spatial-frequency domain.

Considering one harmonic component of the road profile $q(X,k) = Q_0(k)e^{ikX}$, characterised by angular-spatial-frequency $k = 2\pi/\lambda$, where λ is the wavelength of disturbances [23], the effective road profile associated with this harmonic can be obtained:

$$q_e(X,k) = \frac{1}{2a}\int_{X-a}^{X+a} Q_0(k) e^{ik\tilde{X}} d\tilde{X} \tag{6}$$

Integrating:

$$q_e(X,k) = \frac{1}{2a}\frac{Q_0(k)}{ik}[e^{ika} - e^{-ika}]e^{ikX} = Q_{0e}(k)e^{ikX} \tag{7}$$

The filter transfer function can be calculated:

$$H(k) = Q_{0e}(k)/Q_0(k) \tag{8}$$

which, after transforming complex exponentials, yields:

$$H(k) = \frac{\sin(ka)}{ka} \tag{9}$$

This transfer function represents a low-pass filter with a series of zeros for $k = n\pi/a$, with $n \in \mathbb{N}^+$ [24]. The first zero appears for a wavelength equal to the length of the contact patch ($k = 2\pi/2a$).

Wheelbase filtering

While the bicycle is travelling straight on an uneven road, the same road disturbance first excites the front wheel and then the rear wheel with a time delay w/V, where w is the bicycle wheelbase, and V is the constant forward speed. In the time domain, if the vertical displacement under the front wheel due to road unevenness is $z(t)$, the vertical displacement under the rear wheel is $z(t - w/V)$, see Figure 2. This phenomenon is known as wheelbase filtering [14,25,26]. In the frequency domain, this relationship is expressed by the time shift property of the Fourier transform [27]: if $Z(\omega)$ is the Fourier transform of $z(t)$, with ω being the angular frequency, the transforms of front and rear excitations are:

$$\begin{bmatrix} Z_f \\ Z_r \end{bmatrix} = \begin{bmatrix} Z(\omega) \\ Z(\omega)e^{-i\omega\frac{w}{V}} \end{bmatrix}. \tag{10}$$

Figure 2. Wheelbase filtering.

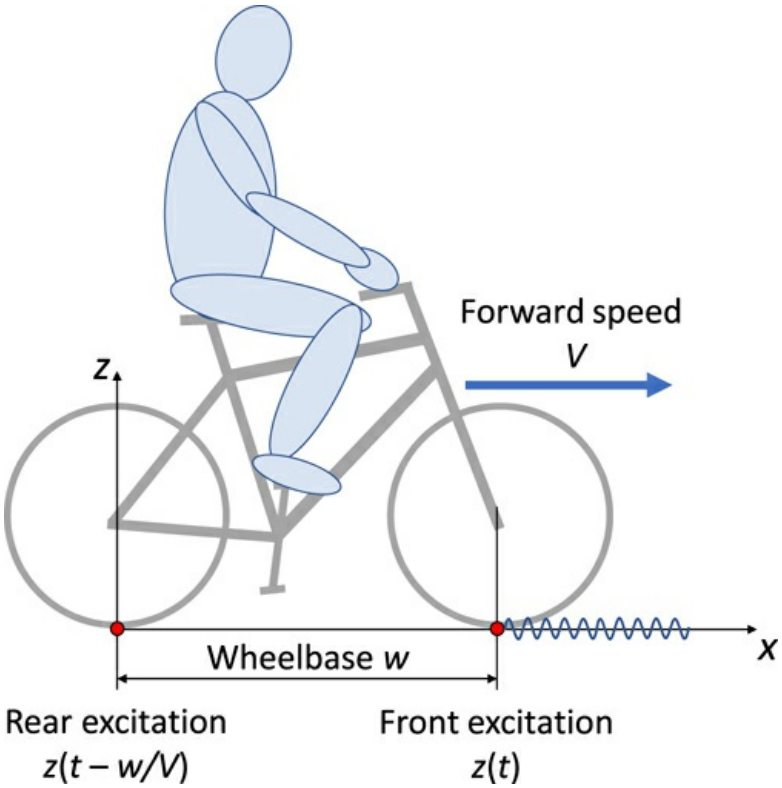

If the bicycle is assumed to have a linear behaviour, a component $A(\omega)$ of the acceleration of a sensitive point of the bicycle (*e.g.* the handlebar or the saddle [26]) can be calculated making use of the frequency response functions (FRFs) between the acceleration component of this sensitive point, and front and rear excitation, $FRF_f(\omega)$ and $FRF_r(\omega)$ respectively. The global response of the sensitive point to road excitation can be obtained summing the contributions of front and rear excitations:

$$A(\omega, V) = \left(FRF_f(\omega) + FRF_r(\omega)e^{-i\omega\frac{w}{V}}\right) Z(\omega) = FRF^*(\omega, V)Z(\omega), \tag{11}$$

where $FRF^*(\omega, V)$ is called correlated FRF and takes into account the interference between front and rear excitation due to wheelbase filtering. The correlated FRF defines how vibrations are transmitted from the road to the sensitive point and can be used to predict comfort on the road once road excitation is appropriately described. This approach cannot model non-linear effects that may be present in shock absorbers (*e.g.* different damping coefficients in bound and rebound, and dry friction [28]).

Vibrations of the sensitive points

In order to estimate the vibrations of the sensitive points, a road profile represented as a standardised PSD [13] is considered. The tyre-road interaction filter is applied to the road PSD, obtaining an effective road input [15,29], which is the input of the bicycle model consisting of the correlated FRF.

According to the ISO 8608 standard [13], the PSD of the road profile (S_{rr}) as a function of the angular-spatial-frequency k, is represented by:

$$S_{rr}(k) = S_0 \left(\frac{k}{k_0}\right)^{-2}, \tag{12}$$

where S_0 is the coefficient that expresses road quality ($S_0 \in [2,8] \cdot 10^{-6}\,\mathrm{m^3/rad}$ for a B-class ISO road) and $k_0 = 1\,\mathrm{rad/m}$ is the reference angular spatial frequency.

The effective road PSD, $S_{rr,e}$, is calculated from the standardised road PSD, S_{rr}, using the transfer function of the filter H, presented in Equation (9):

$$S_{rr,e}(k) = S_{rr}(k)|H(k)|^2. \tag{13}$$

Since the correlated FRF depends on frequency ω and forward speed V, the road PSD has to be expressed in the frequency domain (instead of the angular-spatial-frequency domain) as follows [23]:

$$S_{rr,e}(\omega, V) = \frac{S_{rr,e}\left(k = \frac{\omega}{V}\right)}{V}. \tag{14}$$

This description of the road profile makes it possible to predict the PSD of an acceleration component of the sensitive point of the bicycle (R_{aa}) using the modulus of the correlated FRF:

$$R_{aa}(\omega, V) = |FRF^*(\omega, V)|^2 S_{rr,e}(\omega, V). \tag{15}$$

As both the road PSD and the correlated FRF depend on the forward speed V, the vehicle response is speed dependent. A cyclist typically rides with varying speed, so the use of the statistical concept of vehicle mission is required for comfort assessment [14]. A vehicle mission consists of a probability density function of speed $P(V)$, which represents the probability of forward speed V taking a particular value in the interval $[V_{min}, V_{max}]$. The vehicle mission makes possible the calculation of the average PSD of an acceleration component as follows:

$$\bar{R}_{aa}(\omega) = \int_{V_{min}}^{V_{max}} R_{aa}(\omega, V)\, P(V)\, dV. \tag{16}$$

A simple way to summarise the results and assess the level of comfort perceived by the rider is calculating the root mean square value (RMS) of an acceleration component of the sensitive point. This acceleration index is a comfort indicator and can be computed by integrating $\bar{R}_{aa}(\omega)$ over the frequency range of interest:

$$A_I = \sqrt{\int_0^{\omega_{max}} \bar{R}_{aa}(\omega) w^2(\omega) d\omega}\,. \tag{17}$$

In order to obtain a more meaningful index, the average PSD of the acceleration of the sensitive point can be multiplied by the weighting function $w(\omega)$, which accounts for human sensitivity to whole-body vibrations and hand-transmitted vibrations according to ISO 2631–1 [30] and ISO 5349–1 [31], respectively. It is worth noticing that the seated posture considered by international standards is only an approximation of the actual posture of a rider on a bicycle.

Experimental methods

Laboratory tests

The laboratory methodology consists in exciting the bicycle tyres by means of acceleration impulses and measuring the accelerations transmitted to the sensitive points (*i.e.* seatpost and steerer tube). To perform this test, the bicycle is placed on two tables, as presented in Figure 3, with each wheel centred on the corresponding table. One table is mounted on elastic mounts and is excited by a hammer for modal testing. Due to the hammer hit, this table vibrates and behaves as a simple shaker. The other

table is mounted on rigid mounts and is only needed to guarantee a levelled configuration and to avoid displacements caused by gravity forces. Accelerometers are located on the vibrating table (under the tyre-table contact patch) to measure the input acceleration, and on the sensitive points to measure the output acceleration.

Figure 3. Scheme of the set-up for laboratory tests.

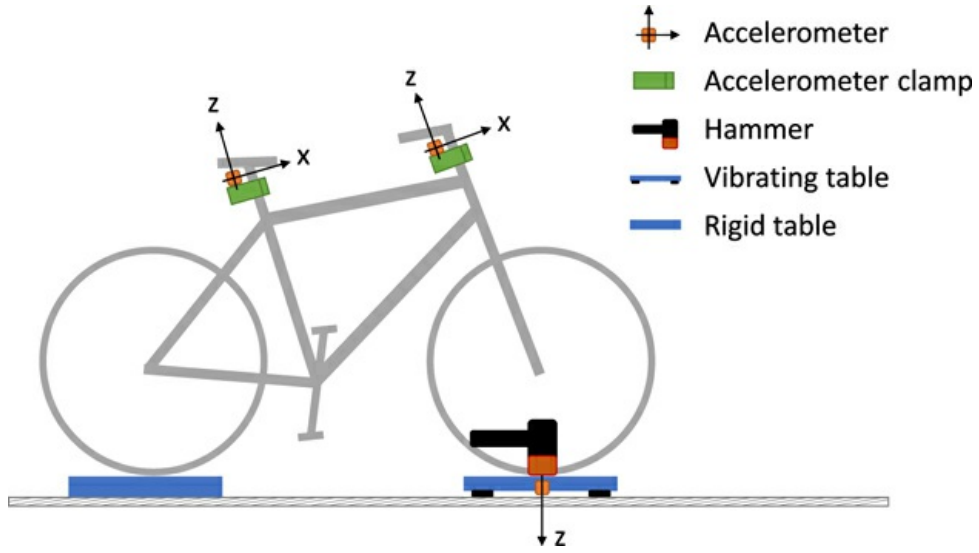

Since normal riding on asphalt bicycle lanes is considered, road excitation is chiefly in the vertical direction, and only the vertical component of the vibrating table acceleration needs to be measured. Vertical excitation of the tyre can cause bicycle vibrations in all directions, owing to the shape of vibration modes. In straight running, the most important components are in the longitudinal plane. Therefore, a triaxial accelerometer is used to measure the acceleration components of the sensitive points in the longitudinal plane, see Figure 3.

The true sensitive points are the handles and the saddle, but it is very difficult to embed a triaxial accelerometer in these parts of the bicycle. Moreover, the measured accelerations would be strongly affected by the rider and by the materials of these parts, which may exhibit a non-linear behaviour. For these reasons, two sensitive points that allow a simpler mounting of the accelerometer and that are less affected by bicycle parts are chosen.

A custom-made clamp is used to attach the accelerometers to each sensitive point. For the sensitive point related to the saddle, the triaxial accelerometer is fixed to the seatpost, as close as possible to the saddle. The z axis is parallel to the geometric axis of the seatpost, and the x axis is perpendicular to the axis of the seatpost and in the forward motion direction. For the sensitive point related to the handlebar, the triaxial accelerometer is fixed to the steerer tube using the same clamp, with the z and x axes parallel and perpendicular to the steerer tube axis, respectively. With this choice, the x and z axes of the accelerometer are slightly tilted with respect to the longitudinal and vertical axes of the bicycle. However, it is worth noticing that, for a seated posture, international standards state that the measurement direction of whole-body vibrations should be determined by the axis of the body, and that the z axis will not necessarily be vertical [30,32]. Hand-transmitted vibrations are defined either with respect to an anatomical coordinate system or with respect to a basicentric coordinate system centred on the vibrating surface [31,32]. Therefore, considering the typical posture of the rider on a bicycle, neither the fixed vertical, horizontal and lateral axes, nor the selected axes are aligned to the axes suggested by international standards. The orientation of accelerometers according to international standards would require a complex and adjustable fixture; conversely, the use of the clamp is a simpler solution, suitable to any bicycle.

The longitudinal movement of the bicycle is prevented by locking the rear brake; preliminary tests showed that this setting improves the repeatability of the tests, without affecting bicycle response. Indeed, locking only the rear wheel prevents fore-aft rigid motions due to rolling about the testing position, but does not alter the modes of vibration, even those with small variations in bicycle wheelbase.

The riders are instructed to ride the bicycle in a relaxed way, without applying unnecessary pressures. Two different solutions are adopted to guarantee the vertical equilibrium of rider and bicycle in indoor tests. In the first solution, the bicycle is held in vertical equilibrium by the rider having one elbow in contact with a flat vertical surface. In the second solution, the rider rests the feet on two small lateral supports, having the same height as the bottom bracket. The first solution does not alter the distribution of weight forces, but constraints a bit the motion of the handlebar. With the second solution, the weight of the feet and lower legs does not load the bicycle. The riders are allowed to choose the configuration ~~in which~~ they feel more natural and comfortable.

In this research, excitation is performed by means of a hammer equipped with a force sensor (PCB 086D20, sensitivity: 0.23

mV/N). The acceleration of the vibrating table is measured by means of a uniaxial piezoelectric accelerometer (PCB 352C22, sensitivity: 1 mV/(m/s^2)). The acceleration components of the sensitive points are measured by means of a triaxial piezoelectric accelerometer (PCB 356A17, sensitivity: 51 mV/(m/s^2)). The FRFs are obtained from the acceleration signals by acquiring the data with an input module for sound and vibration (NI9234). For each input-output point combination, the FRF between the acceleration of the sensitive point (in x or z direction) and the input acceleration is calculated averaging data obtained from 20 hammer hits.

The posture of the rider is verified during the tests by locating non-reflective markers on the rider and the bicycle to characterise the position of different body segments in the sagittal plane. A digital camera is positioned in a plane perpendicular to the cyclist's sagittal plane to register the video of the tests. The head (θ_H), elbow (θ_E), trunk (θ_T) angles, depicted in Figure 4, are measured.

Figure 4. Scheme of the position of markers and angles used for posture verification.

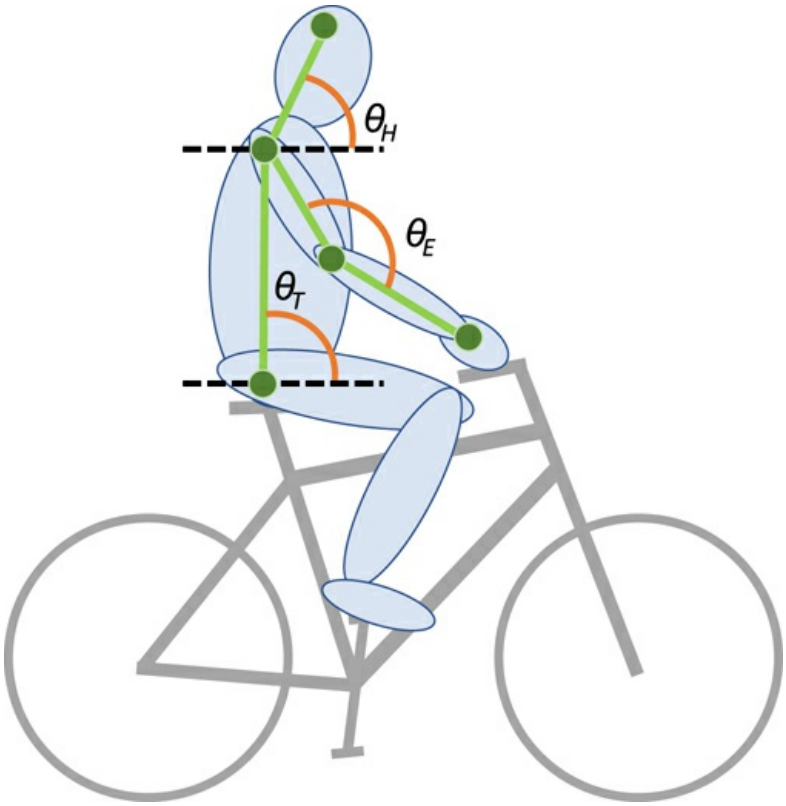

The calculation of the effective road profile (Equation 7) requires an estimate of the contact patch half-length (a). A direct measurement of this parameter from a tyre print may lead to large errors. Therefore, the shape of the contact patch is identified from a set of tests in which the print of the patch generated by each tyre on the ground is digitalised. Given a picture of an arbitrary patch, the identification model assumes that the contour can be represented as a super-ellipse. This model has been previously used for the representation of contact patches of other road vehicles due to its capability of describing different shapes and sizes [33]. In an orthonormal coordinate system, the super-ellipse is described by three parameters (a, b, n) as:

$$\left(\frac{x}{a}\right)^n + \left(\frac{y}{b}\right)^n = 1, \tag{18}$$

where $n \in \mathbb{R}^+$ is the exponent of the expression. a and b correspond to half of the length of the major axes of a super-ellipse that is centred in the origin and has its major axes parallel to the axes of the coordinate system. To complete the identification of the contact patch, it is necessary to consider a rotation and a translation in the plane, which are defined by three parameters.

The identification process is based on the minimisation of a cost function that compares the super-ellipse associated with a set of parameters with the measured contact patch. The cost function is defined by the sum of the total area of false-positives and the total area of false-negatives. A section of area is considered as false-positive if it is inside the region defined by the super-ellipse, but it is not a part of the measured contact patch. Analogously, a section of area is considered as false-negative if it is outside of the region defined by the super-ellipse, but it is part of the original contact patch.

The identification process is completed by selecting the set of parameters that minimises the cost function. Figure 5 presents an example of the superposition of the result of the identification process on the corresponding original picture.

Figure 5. Example of the contact patch's identification.

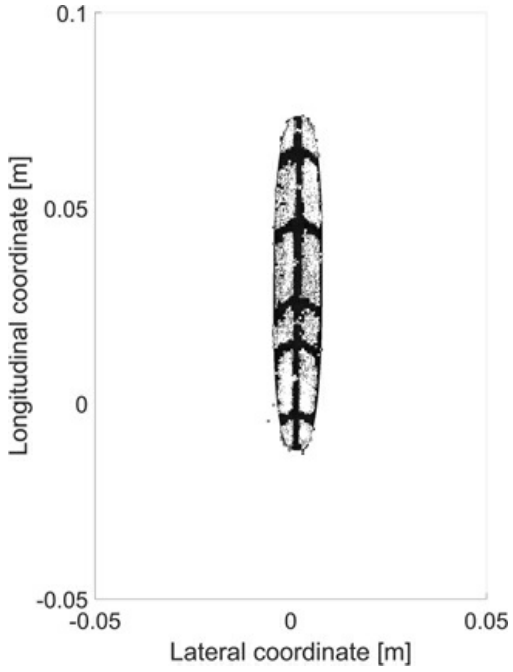

Road tests

The road tests are performed riding the bicycle on a given road segment, pedalling continuously, and aiming at maintaining constant target speeds and measuring the vibrations of the sensitive points. The road data is acquired with triaxial accelerometers (Mide SlamStick LOG-0003-16G-8GB-PC, resolution 0.04 m/s^2) located on the steerer tube and seatpost as presented in Figure 3, using the same clamp employed in the laboratory tests. A GPS based speed sensor is used to register the bicycle speed. The speed is displayed to the rider in real-time through a handlebar-mounted screen, as an aid to maintain the target speed; moreover, the speed time history is saved to be used in subsequent analyses. The tests are performed on a 150 m, straight, flat, asphalted bicycle lane, and three trials are performed for each testing speed.

Tested bicycles and riders

The tests were performed for two bicycle-cyclist sets. Bicycle 1 is a basic diamond-frame city bicycle (steel frame, tyres: ERTRO 37–622, inflation pressure: 3.0 bar, wheelbase: 1.07 m, head tube angle 70°, seat tube angle 73°). Bicycle 2 is a basic step-through-frame city bicycle (steel frame, tyres: ERTRO 37–590, inflation pressure: 3.0 bar, wheelbase: 1.05 m, head tube angle 70°, seat tube angle 73°).

The laboratory and road tests were performed by two male riders who voluntarily participated in the study (rider of Bicycle 1: mass: 73 kg, height: 193 cm, age: 26 years; rider of Bicycle 2: mass: 65 kg, height: 172 cm, age: 59 years).

Analysis of laboratory tests results

The acceleration-acceleration FRFs measured in laboratory were multiplied by the squared angular frequency to obtain the acceleration-displacement FRFs to be used as input in Equation 11. The frequency analysis was carried out in the 0-100 Hz range considering the purpose of the analysis. Figure 6 shows the acceleration-displacement FRFs registered for Bicycle 1 and 2 for the four excitation and sensitive point combinations. Each FRF was obtained as the average of the results of 20 hammer hits. Some features associated with the vibration modes of the bicycle can be observed. The peaks in the 10-50 Hz range are related to the modes of vibration dominated by tyre deformation and to the first structural modes of front and rear assembly [34]. The narrow peak at 60 Hz in the FRFs of Bicycle 2 with front excitation corresponds to a structural mode of the frame (typical of the step-through design) with large relative motions between the saddle and the handlebar (*i.e.* scissor mode [34]). In general, the bandwidths around the resonances of Bicycle 2 are larger than the ones of Bicycle 1.

Figure 6. Measured acceleration-displacement FRFs. (a) Bicycle 1. (b) Bicycle 2.

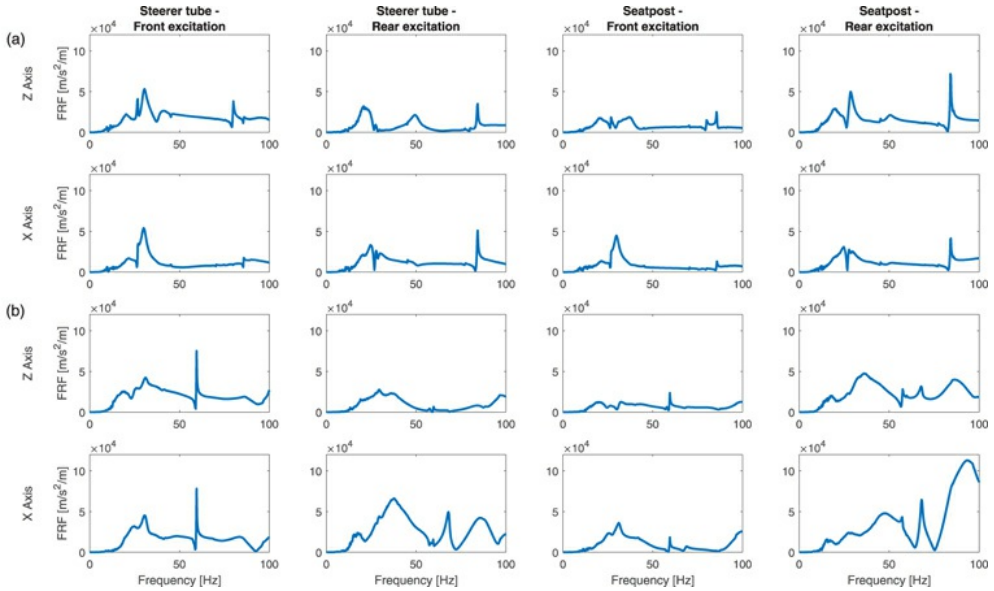

One of the advantages of laboratory tests compared to road tests is the better control and monitoring of the rider's posture. Figure 7 presents the distribution of the upper body angles of the cyclist during the laboratory tests. The posture of the cyclist on both bicycles was similar. The difference in the angles of the elbow and trunk can be attributed to the change in the bicycle geometry. In terms of repeatability, the postural angles of trunk and elbow exhibit low dispersions; this is justified by the posture instructions given to the rider, which considered extended arms, thus fixing a closed kinematic chain for the upper body. The head orientation has a higher dispersion, since it is associated with an open kinematic chain.

Figure 7. Posture registered during laboratory tests with bicycles 1 and 2. Average and standard deviation of the measured angles.

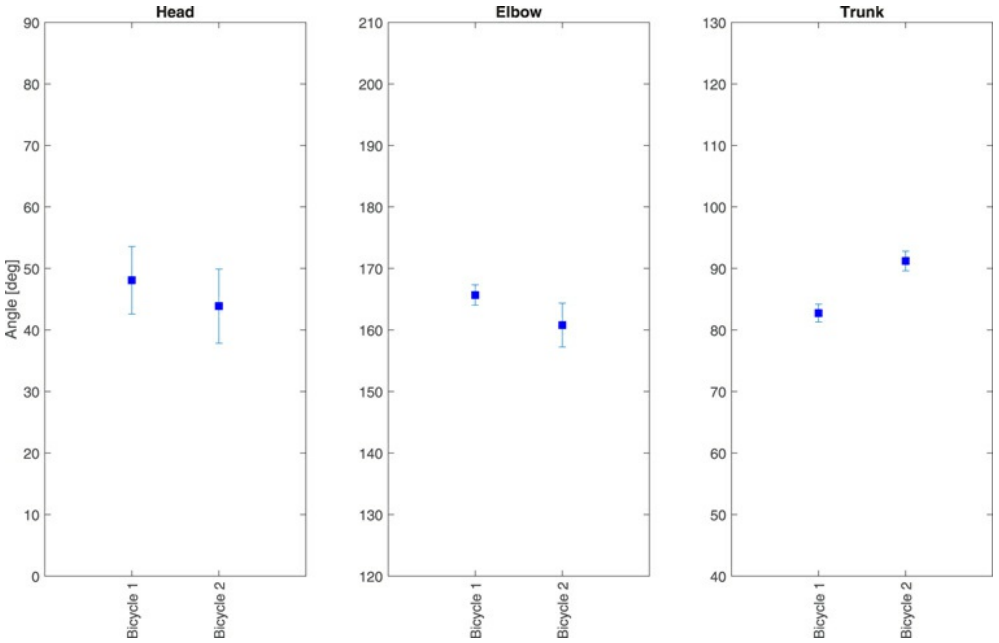

The measured FRFs were elaborated to obtain the correlated FRF of each sensitive point considering the effect of wheelbase filtering. Figure 8 exhibits the correlated FRF obtained for the sensitive points of Bicycle 1 in z direction; similar results can be obtained for the other bicycle and for the x direction. A constant speed of 15 km/h was used to exemplify the numerical elaboration. The lobes caused by wheelbase filtering can be observed in the correlated FRF of both sensitive points. The shape of these lobes changes depending on the speed used for calculation of the correlated FRF.

Figure 8. Correlated FRFs of the sensitive points of Bicycle 1 (example at 15 km/h, z axis).

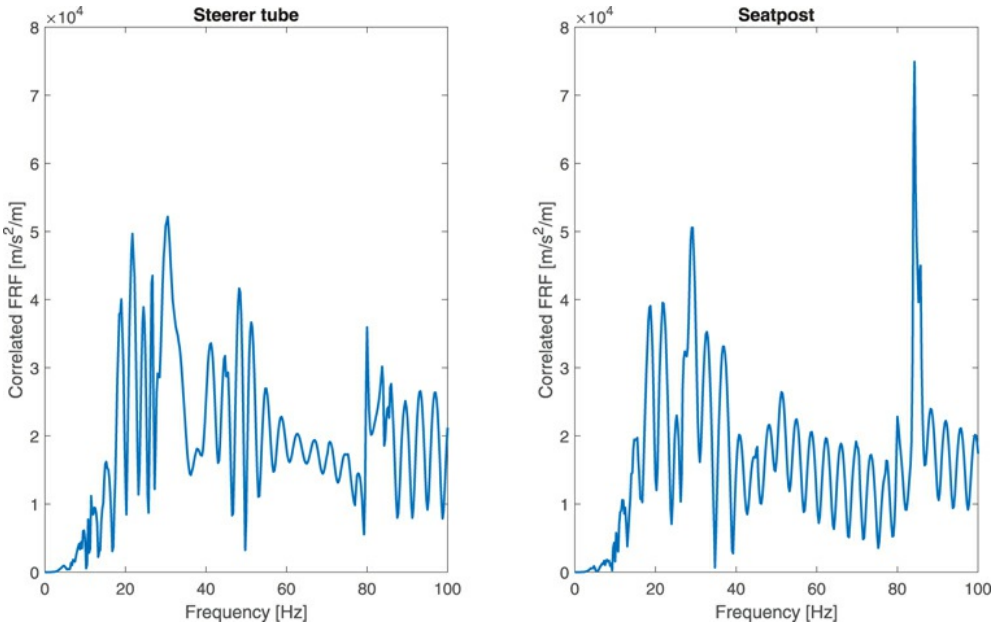

The acceleration PSD of each sensitive point was obtained using the correlated FRF and the effective road PSD as in Equation 15. In this study, a road coefficient $S_0 = 3.5 \cdot 10^{-6}$ m^3/rad was adopted. This value belongs to B-class roads [13] and is representative of the quality of asphalt bicycle lanes in Italy. The low-pass filter described in Equation 9 was used to represent the tyre filtering phenomena. Figure 9 presents the vertical acceleration PSDs calculated for Bicycle 1 with and without the tyre filtering effect. It is worth mentioning that the case in which the tyre filtering effect is neglected corresponds to the condition in which the contact between tyre and road is modelled as a point contact. The results shown in Figure 9 agree with previous studies [19,20,22], in which different tyre models are compared, and where noticeable differences between point contact and flexible tyre model responses are reported over 10 Hz. It is also worth highlighting that, given the tyre filtering effect, the frequency range of interest for the acceleration PSDs of the sensitive points is limited to the 0-50 Hz range. Above the upper bound of this interval, the vibration level is low since the input coming from road perturbations is strongly reduced by the tyre-road interaction.

Figure 9. Acceleration PSDs obtained from correlated FRFs of Bicycle 1 (example at 15 km/h, z axis).

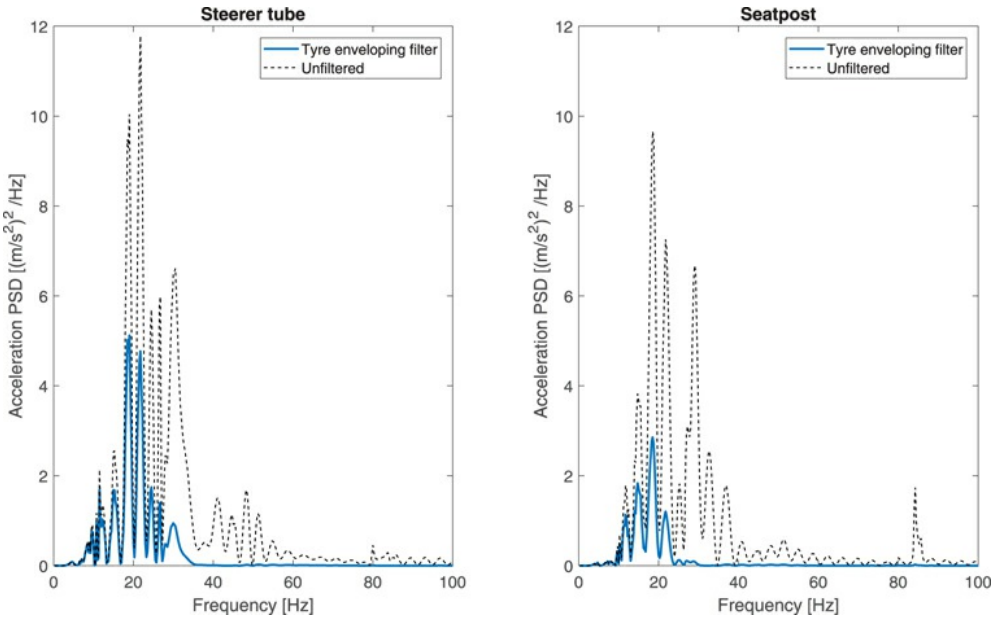

Analysis of road tests results

The road tests were performed at three target speeds, selected according to the typical speed range of a city bicycle: 10, 15, and 20 km/h. During the road tests, acceleration and speed data were acquired, synchronising them with a starting trigger. As the tests were planned with a given target speed, the data was segmented into trials; each trial was defined as the interval in which the speed differs by less than 10% from the actual average speed. Three trials were performed for each testing speed. The segmentation process is exemplified in Figure 10.

Figure 10. Example of road test data segmentation into trials at constant speed (Bicycle 1, steerer tube, nominal speed of 15 km/h). (a) Acceleration signal. (b) Speed signal and speed average for each trial.

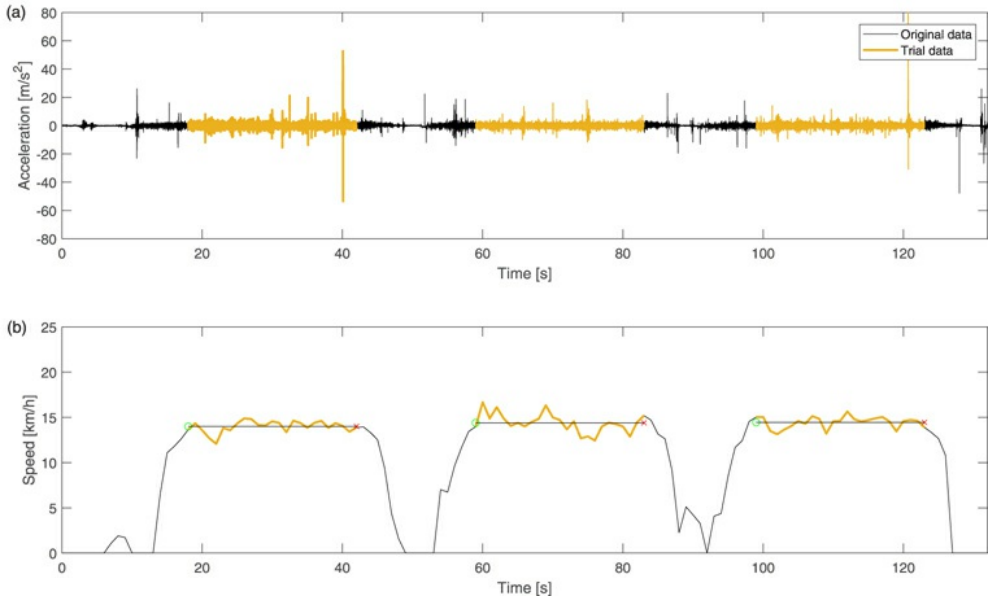

The variation of speed with respect to the target value has to be taken into account in the subsequent comparison between road results and laboratory predictions. For this purpose, the speed signals recorded during the road tests were used to compute a Gaussian vehicle mission to be used in the mathematical model of the proposed method. The mean and standard deviation of each distribution, fitted with a Gaussian probability function, are calculated from time-domain data of the three trials and are reported in Table 1.

Table 1. Vehicle mission parameters calculated from road test speed signals.

BICYCLE	BICYCLE 1			BICYCLE 2		
TARGET SPEED (km/h)	10	15	20	10	15	20
MEAN (km/h)	9.6	14.6	19.0	12.0	14.6	16.0
STD. DEV. (km/h)	0.58	0.72	1.05	1.01	2.50	2.61

The PSDs of the acceleration components were obtained from the road data using the Welch algorithm [35]. For each sensitive point, the results were filtered to consider human body sensitivity to vibrations according to ISO 5349–1 [31] and ISO 2631–1 [30] for hands and whole-body, respectively. Figures 11–14 present road tests results.

Figure 11. Average PSDs obtained from road tests and laboratory tests at different speeds, considering human sensitivity: Bicycle 1, z axis.

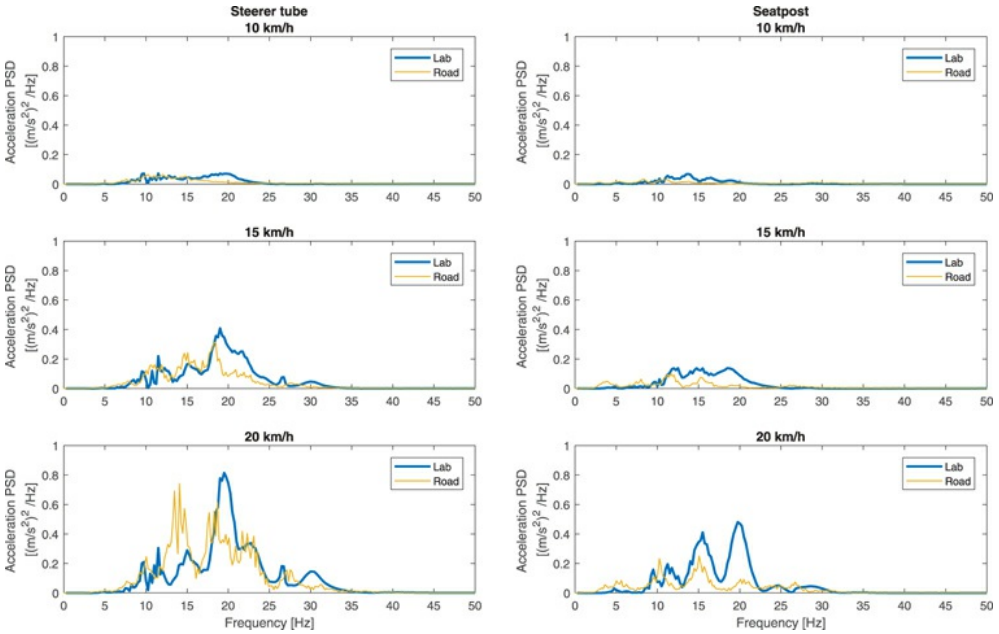

Figure 12. Average PSDs obtained from road tests and laboratory tests at different speeds, considering human sensitivity: Bicycle 1, x axis.

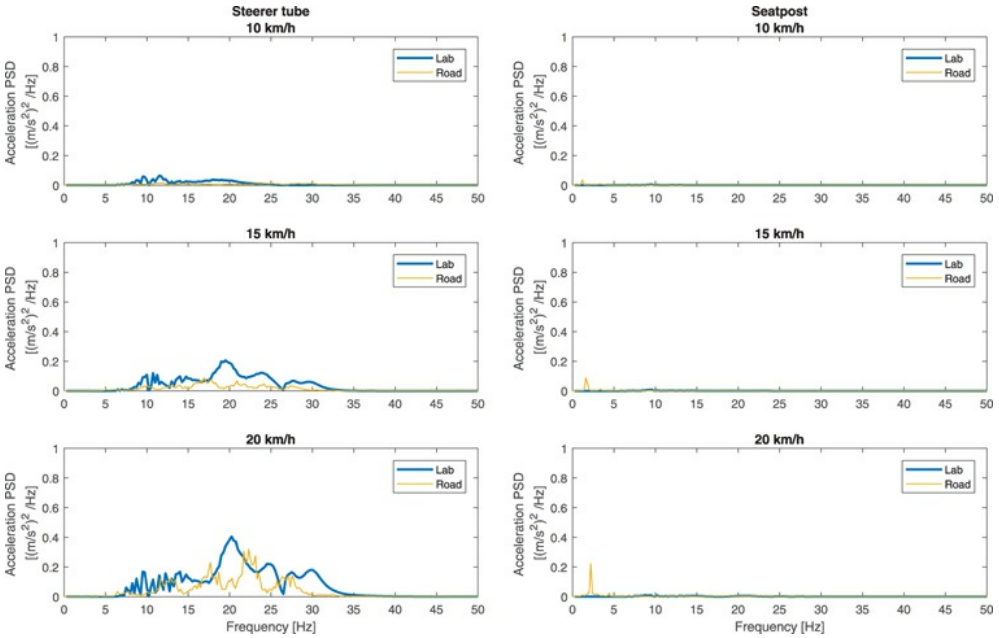

Figure 13. Average PSDs obtained from road tests and laboratory tests at different speeds, considering human sensitivity: Bicycle 2, z axis.

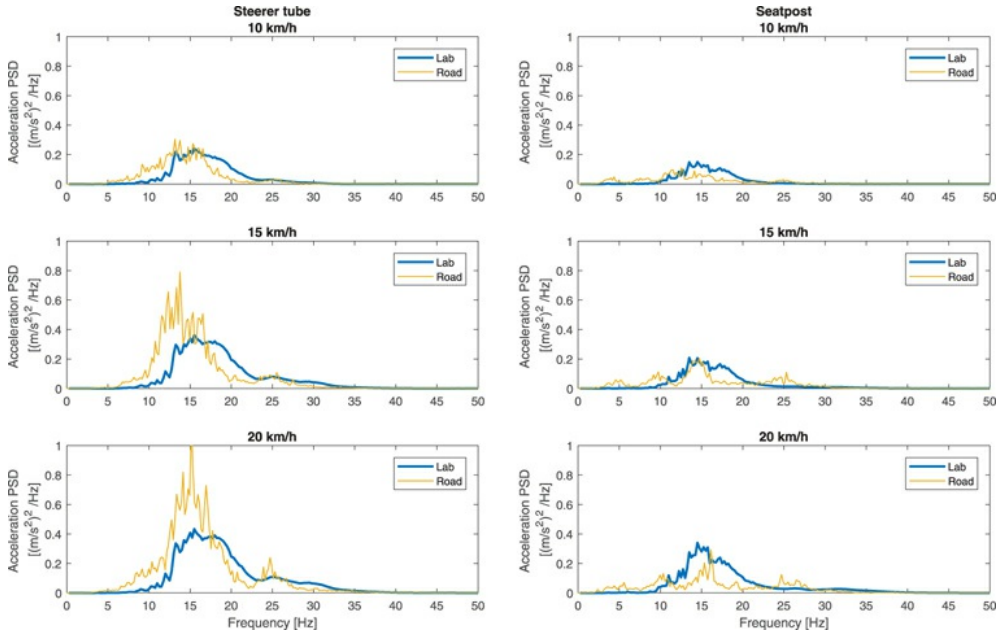

Figure 14. Average PSDs obtained from road tests and laboratory tests at different speeds, considering human sensitivity: Bicycle 2, x axis.

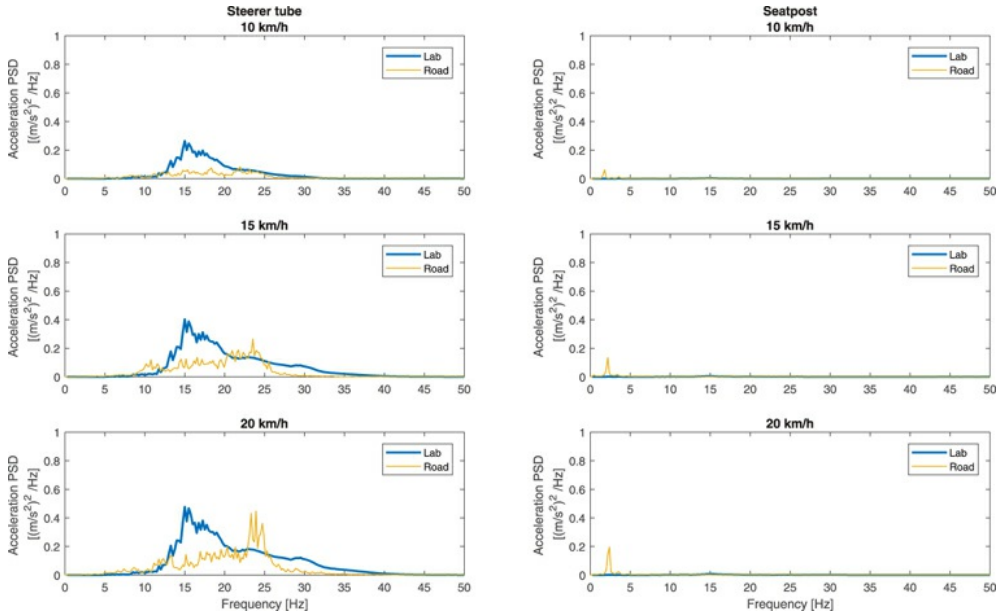

For both bicycles, the main peaks of acceleration PSDs appear in the range 10-30 Hz. Amplitudes tend to vanish above 30 Hz; this effect is caused by tyre filtering and human sensitivity. In both sensitive points and in both directions, the acceleration amplitudes increase with speed. Considering the z direction, the largest accelerations are measured at the steerer tube in both bicycles. Considering the x direction, both bicycles show relevant amplitudes at the steerer tube and negligible amplitudes at the seatpost.

The main difference between the PSDs measured for the two bicycles is that the rider of Bicycle 1 was able to keep the speed more constant, and the typical peaks caused by wheelbase filtering are evident in Figures 11 and 12. Conversely, the rider of Bicycle 2 caused larger speed variations during the road tests, which reflect in higher standard deviations of the corresponding Gaussian probability density functions, see Table 1. This effect averaged the narrow peaks typical of wheelbase filtering at a constant speed, see Figures 13 and 14.

Comparison between laboratory predictions and road tests results

The PSDs of the components of acceleration of the sensitive points were obtained from the laboratory tests for the same conditions of the road tests. The vehicle missions used for the estimation were defined taking as input the speed distribution registered during the road tests and fitting it with Gaussian probability density functions, see Table 1. Figures 11–14 present the comparison between the PSDs obtained from road tests and laboratory tests for both tested bicycles and directions, and for three speeds. The experimental-numerical method based on laboratory tests is able to predict the most important features of road results. In particular, even if there are some differences, the PSDs derived from laboratory tests show the largest amplitudes in the same frequency bands as road tests, correctly predict the increase in acceleration amplitude with speed, highlight that the

maximum acceleration takes place at the steerer tube in z direction, and point out that that x acceleration is relevant at the steerer tube and negligible at the seat-post.

For Bicycle 1 in z and x directions there is a good agreement between the peak frequencies and sometimes between the peak values obtained with the two methods. For Bicycle 2, in z direction there is a rather good agreement between the peak frequencies obtained with the two methods. The agreement between the peak amplitudes decreases when speed increases. In x direction the peaks obtained with the two methods are in the same band and have similar values, but are not coincident.

These differences may be caused by some phenomena that are present on the road but are not considered in laboratory tests. On the road, due to the active state of the rider, the body posture may differ from the one adopted during the laboratory tests [8,36]. Even if the quality of the bicycle lane is good, the presence of small localised defects that generate impulsive excitations is unavoidable. These strong and short excitations may cause a non-linear response of the bicycle. The trajectory of the bicycle is not perfectly straight, because the bicycle lane is public, and sometimes the rider has to correct the trajectory to cope with the presence of other bicycles.

In order to further compare laboratory tests results with road tests results, the acceleration indices for the two directions were computed according to Equation 17. Figures 15 and 16 show the results of these calculations. For road tests, the mean values and the standard deviations (estimated considering the dispersion of the acceleration indices calculated for each trial) are presented. For laboratory tests, the standard deviation is not meaningful, since accelerations were predicted from average FRFs obtained from 20 excitations. The analysis of Figures 15 and 16 shows a good agreement between the two sets of results. In most cases, the difference between the indices obtained with the two methods is not too large when compared with the standard deviation of road tests results. The two sets of acceleration indices show the same dependence on speed. There is no general trend, but usually, the laboratory tests predict larger acceleration indices than road tests, with the exception of z acceleration of the steerer tube of Bicycle 2.

Figure 15. Comparison of acceleration indices obtained from road and laboratory tests at different speeds, considering human sensitivity: Bicycle 1.

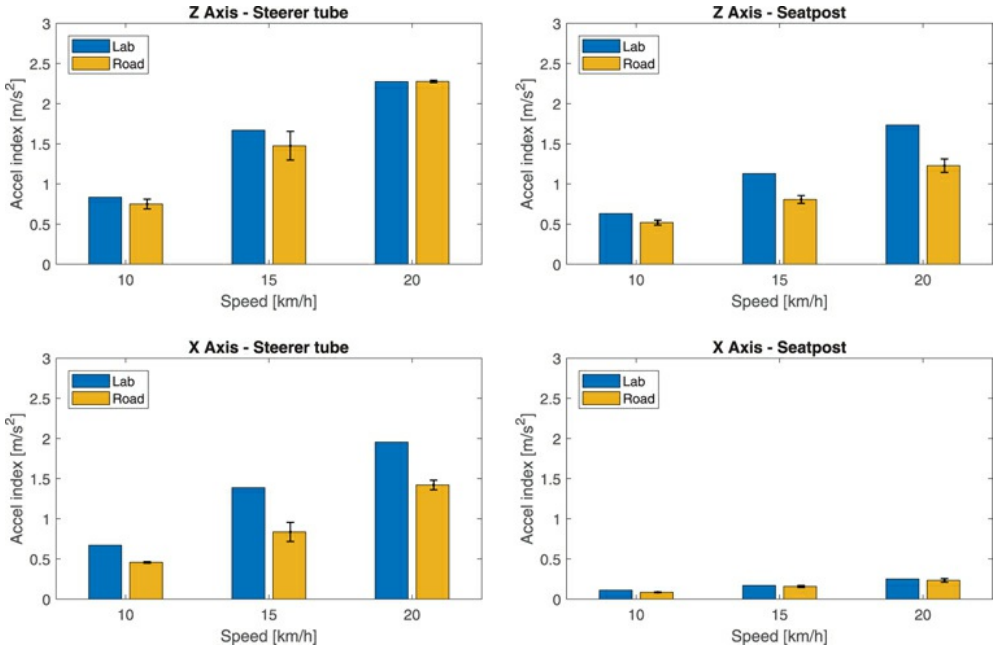

Figure 16. Comparison of acceleration indices obtained from road and laboratory tests at different speeds, considering human sensitivity: Bicycle 2.

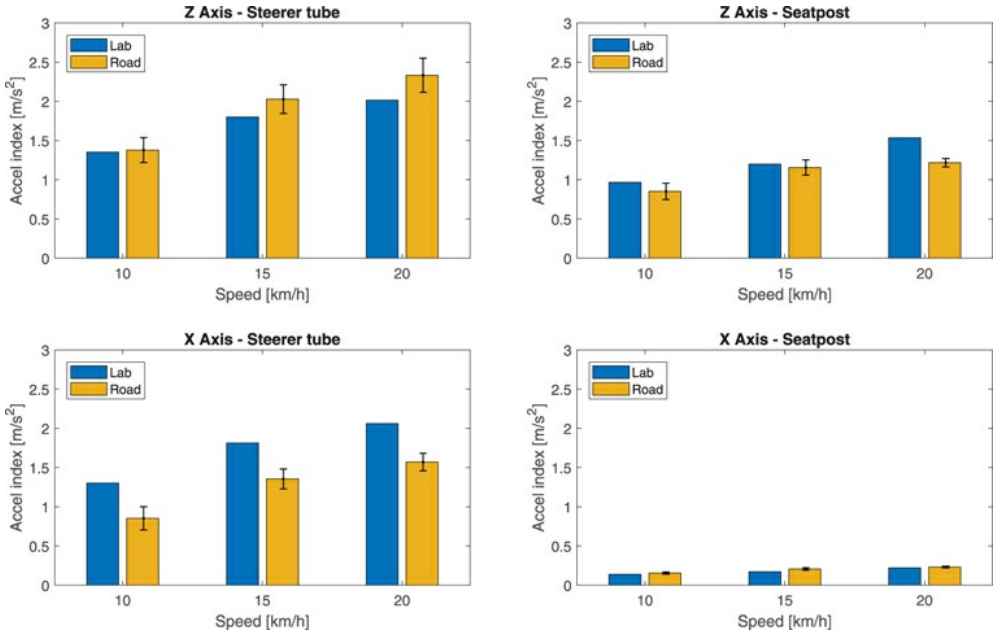

It is worth highlighting that the results of the laboratory tests depend on the road quality, among others. For this study, the road quality was defined considering the usual conditions of Italian bicycle lanes. For this reason, the results could be improved by measuring the road roughness of the lanes in which the road tests are performed.

Conclusion

The proposed laboratory testing method for the prediction of on-road comfort of city bicycles is rather simple, does not require expensive equipment, and it permits to measure the rider's posture. The combination of the measured FRFs and a numerical code that considers wheelbase and tyre filtering makes it possible to estimate the comfort properties of the bicycle on the road.

The comparison between the acceleration indices calculated from laboratory tests and road tests shows a general agreement. The comparison between the acceleration PSDs of the sensitive points obtained with the two approaches shows that the experimental-numerical method is able to replicate the most important features of road tests results.

The proposed method can be usefully applied in different scenarios. From a single set of laboratory tests, the effect of different vehicle missions (*i.e.* bicycle speeds) or different road qualities on comfort can be assessed. This characteristic of the proposed method can lead to relevant reductions in the testing time. Moreover, the proposed method can be used to rank the comfort properties of different bicycles.

Acknowledgements

This research was partially supported by the Colombian Administrative Department of Science, Technology, and Innovation (COLCIENCIAS) under Grant 727-2015.

Disclosure statement

No potential conflict of interest was reported by the authors **[Q1]**.

ORCID

Edoardo Marconi http://orcid.org/0000-0001-8221-4472

Alejandra Polanco http://orcid.org/0000-0002-9561-6443

References

1 **Ayachi S, Dorey J, Guastavino C.** Identifying factors of bicycle comfort: An online survey with enthusiast cyclists. Appl Ergon. 2015;46:124–136. DOI: 10.1016/j.apergo.2014.07.010 .

2 **Olieman M, Marin-Perianu R, Marin-Perianu M.** Measurement of dynamic comfort in cycling using wireless acceleration sensors. Procedia Eng. 2012;34:568–573.

3 **Giubilato F, Petrone N.** A method for evaluating the vibrational response of racing bicycles wheels under road roughness excitation. Procedia Eng. 2012;34:409–414.

4 **Pelland-Leblanc J, Lépine J, Champoux Y, et al.** Using power as a metric to quantify vibration transmitted to the cyclist. Procedia Eng. 2014;72:392–397.

5 **Chiementin X, Crequy S, Feron R, et al.** Contribution of bamboo for vibratory comfort in biomechanics of cycling. The Open Mechanical Eng J. 2017;11:44–54. DOI: 10.2174/1874155X01711010044.

6 **Roa S, Muñoz L.** An experimental methodology for evaluating the energy cost and comfort during cycling: A case study for analyzing tyre pressure influence. Vibroengineering Procedia. 2015;5:552–557.

7 **Lépine J, Champoux Y, Drouet J.** Test protocol for in-situ bicycle wheel dynamic comfort comparison. Procedia Eng. 2016;147:568–572.

8 **Lépine J, Champoux Y, Drouet J.** Road bike comfort: On the measurement of vibrations induced to cyclist. Sports Eng. 2014;17(2):113–122. DOI: 10.1007/s12283-013-0145-8 .

9 **Petrone N, Trabacchin F.** 2014. Development of a test bench for the subjective and objective evaluation of the vibrational comfort of bicycle components. In: ASME 2014 International Design Engineering Technical Conferences and Computers and Information in Engineering Conference; 2014 Aug 17-20; Buffalo, NY.

10 **Cossalter V, Doria A, Basso R, et al.** Experimental analysis of out-of-plane structural vibrations of two-wheeled vehicles. Shock Vib. 2004;11(3-4):433–443. DOI: 10.1155/2004/905629 .

11 **Ewins D.** Modal testing: theory, practice and application. Baldock (Hertfordshire): Research Studies Press LTD; 2000.

12 **Doria A., Formentini M**. 2011. Identification of the structural modes of high performance bicycles in the perspective of wobble control. In: ASME 2011 International Design Engineering Technical Conferences and Computers and Information in Engineering Conference; 2011 Aug 28-31; Washington, DC.

13 **ISO 8608**. Mechanical vibration - road surface profiles - Reporting of measured data. Geneva: International Organization for Standardization; 2016.

14 **Cossalter V, Doria A, Garbin S, et al.** Frequency-domain method for evaluating the ride comfort of a motorcycle. Veh Syst Dyn. 2006;44(4):339–355. DOI: 10.1080/00423110500420712 .

15 **Guo K, Liu Q.** 1998. A model of tyre enveloping properties and its application on modelling of automobile vibration systems. SAE Technical Paper 980253; 1998.

16 **Taheri S, Sandu C, Taheri S, et al.** A technical survey on terramechanics models for tyre–terrain interaction used in modeling and simulation of wheeled vehicles. J Terramechanics. 2015;57:1–22. DOI: 10.1016/j.jterra.2014.08.003 .

17 **Zegelaar P, Pacejka H.** The in-plane dynamics of tyres on uneven roads. Veh Syst Dyn. 1996;25(S1):714–730.

18 **Brinkmeier M, Nackenhorst U, Petersen S, et al.** A finite element approach for the simulation of tyre rolling noise. J Sound Vib. 2008;309(1-2):20–39. DOI: 10.1016/j.jsv.2006.11.040 .

19 **Múčka P, Gagnon L.** Influence of tyre–road contact model on vehicle vibration response. Veh Syst Dyn. 2015;53(9):1227–1246. DOI: 10.1080/00423114.2015.1041992 .

20 **Captain K, Boghani A, Wormley D.** Analytical tyre models for dynamic vehicle simulation. Veh Syst Dyn. 1979;8(1):1–32. DOI: 10.1080/00423117908968566 .

21 **Dodds C, Robson J.** The description of road surface roughness. J Sound Vib. 1973;31(2):175–183. DOI: 10.1016/S0022-460X(73)80373-6 .

22 **Cebon D.** Heavy vehicle vibration-a case study. Veh Syst Dyn. 1986;15(s1):30–43. DOI: 10.1080/00423118508968791 .

23 **Davis B, Thompson AG.** Power spectral density of road profiles. Veh Syst Dyn. 2001;35(6):409–415. DOI: 10.1076/vesd.35.6.409.2039 .

24 **Li J, Zhang Z, Wang W.** New approach for estimating international roughness index based on the inverse pseudo excitation method. J Transp Eng, Part B: Pavements. 2019;145(1):04018059), DOI: 10.1061/JPEODX.0000093 .

25 **Gillespie TD.** Fundamentals of vehicle dynamics. SAE Technical paper 1992-02-01; 1992.

26 **Doria A, Marconi E.** 2018. A testing method for the prediction of comfort of city. In: ASME 2018 International Design Engineering Technical Conferences and Computers and Information in Engineering Conference; 2018 Aug 26-29; Quebec City, Canada.

27 **de Silva CW.** Vibration: fundamentals and practice. Boca Raton (FL): CRC Press; 2006.

28 **Cossalter V, Doria A, Pegoraro R, et al.** On the non-linear behaviour of motorcycle shock absorbers. Proc of the Inst of Mech Eng Part D: J of Automob Eng. 2010;224(1):15–27. DOI: 10.1243/09544070JAUTO1273 .

29 **Prasad SK, Dayalan P, Balasubramanian R.** Study on correlation of commercial vehicle axle response with road profile for ISO road class categorization and durability analysis. SAE Technical Paper 2018-01-1114; 2018.

30 **ISO 2631-1**. Mechanical vibration and shock - evaluation of human exposure to whole-body vibration. Geneva: International Organization for Standardization; 2016.

31 **ISO 5349-1**. Mechanical vibration – measurement and evaluation of human exposure to hand-transmitted vibration. Geneva: International Organization for Standardization; 2001.

32 **Griffin M.** Handbook of human vibration. London, England: Academic press LTD; 2012.

33 **Hallonborg U.** Super ellipse as tyre-ground contact area. J Terramechanics. 1996;33(3):125–132. DOI: 10.1016/S0022-4898(96)00013-4 .

34 **Doria A, Marconi E, Cialoni P.** 2019. Modal analysis of a utility bicycle from the perspective of riding comfort. In: ASME 2019 International Design Engineering Technical Conferences and Computers and Information in Engineering Conference; 2019 Aug 18-21; Anaheim, CA.

35 **Welch P.** The use of fast Fourier transform for the estimation of power spectra: a method based on time averaging over short, modified periodograms. IEEE T Acoust. 1967;15(2):70–73. DOI: 10.1109/TAU.1967.1161901 .

36 **Polanco A, Marconi E, Muñoz L, et al.** 2019. Effect of Rider Posture on Bicycle Comfort. In: ASME 2019 International Design Engineering Technical Conferences and Computers and Information in Engineering Conference; 2019 Aug 18-21; Anaheim, CA.